Pergamon

Int. J. Heat Mass Transfer. Vol. 38, No. 3, pp. 503–510, 1995

0017–9310/95 $9.50+0.00

0017–9310(94)00180–4

Computer simulation and flow visualization of thermocapillary flow in a silicone oil floating zone

Y. TAO, R. SAKIDJA and S. KOU†

Department of Materials Science and Engineering and Center of Excellence in Solidification Processing Technologies of Engineering Materials, University of Wisconsin, Madison, WI 53706, U.S.A.

(*Received* 29 *November* 1993 *and in final form* 24 *May* 1994)

Abstract—Computer simulation and flow visualization were conducted to study thermocapillary flow in a small zone of silicone oil held between two differentially heated rods. Despite significant zone necking, converting calculated streamlines to flow patterns that could be compared with the observed flow patterns was possible, by incorporating the lens effect of the oil zone. It was found that the lens effect causes the streamlines to appear to shift toward the free surface and away from the top and bottom of the zone. It also causes the vortex to appear to shift upward and outward. The calculated and converted flow patterns agree very well with the observed ones.

INTRODUCTION

Thermocapillary flow in a liquid column held between two vertical, differentially heated rods, which is sometimes called a half zone, has been a subject of significant interest in the microgravity fluid physics community. Under microgravity natural (buoyant) convection becomes very weak and thermocapillary flow, therefore, dominates.

Many computational studies have been conducted to study fluid flow in a floating zone [1–36]. Most of these studies focused on thermocapillary flow, though some of them examined the effect of rotation, the electromagnetic force and externally applied magnetic fields. Many experimental studies have also been conducted to study fluid flow in a floating zone [37–51], most of them focusing on thermocapillary flow again. Comparison between calculated flow patterns with observed ones, however, has been rather rare if any at all. This comparison, in fact, is not possible unless the optical distortions due to the lens effect of the floating zone are taken into account.

For floating zones that are cylindrical in shape, quantitative description of such optical distortions is available [50, 51]. Unfortunately, floating zones are noncylindrical under normal gravity. In fact, they can also be noncylindrical under microgravity. For example, floatings zones during microgravity crystal growth are often noncylindrical since the growth angle [52] is not zero for many materials. Also, floating zones will have to be noncylindrical if the effect of their shape on thermocapillary flow is to be studied. Recently, quantitative description of optical distortions associated with noncylindrical floating zones has become available [53]. This description has been verified against a grid optically distorted by a Plexiglass model of a noncylindrical shape [53].

The main purpose of the present study is to compare, for the first time, flow patterns based on calculated streamlines with flow patterns observed in flow visualization in floating zones that are noncylindrical in shape. Streamlines are first calculated by computer simulation and then converted to flow patterns by considering the lens effect of the floating zone. Flow visualization is then conducted and the observed flow patterns are compared with the calculated and converted ones. Non-axisymmetric oscillatory convection was not observed in flow visualization and is, therefore, not considered here.

GOVERNING EQUATIONS AND BOUNDARY CONDITIONS

The physical system being considered is illustrated schematically in Fig. 1. Convection in the oil zone is assumed axisymmetric, laminar and at the steady state.

Equation of motion

$$\frac{\partial}{\partial r}\left(\frac{\omega}{r}\frac{\partial\psi}{\partial z}\right)-\frac{\partial}{\partial z}\left(\frac{\omega}{r}\frac{\partial\psi}{\partial r}\right)+\frac{\partial}{\partial r}\left[\frac{1}{r}\frac{\partial}{\partial r}(\mu r\omega)\right]+\frac{\partial}{\partial z}\left[\frac{1}{r}\frac{\partial}{\partial z}(\mu r\omega)\right]-\rho_{\mathrm{L}}\beta g\left(\frac{\partial T}{\partial r}\right)=0. \quad (1)$$

Stream equation

$$\frac{\partial}{\partial z}\left[\frac{1}{\rho_{\mathrm{L}}r}\frac{\partial\psi}{\partial z}\right]+\frac{\partial}{\partial r}\left[\frac{1}{\rho_{\mathrm{L}}r}\frac{\partial\psi}{\partial r}\right]+\omega=0. \quad (2)$$

†Author to whom correspondence should be addressed.

NOMENCLATURE

a, b, c, d	coefficients in general governing equation
C_p	specific heat
$\vec{e}_r$	unit vector in r-direction
$\vec{e}_z$	unit vector in z-direction
g	gravitational acceleration
h	heat transfer coefficient
k	thermal conductivity
n	refraction index
$\vec{n}$	unit normal vector
r	radial coordinate
$\vec{s}$	unit tangential vector
$\mathbf{t}$	stress tensor
T	temperature
u	radial velocity component
v	axial velocity component
z	axial coordinate.

Greek symbols

β	thermal expansion coefficient
γ	surface tension
ε	emissivity
η	curvilinear coordinate
μ	dynamic viscosity
ξ	curvilinear coordinate
ρ	density
σ	Stefan–Boltzmann constant
ϕ	general dependent variable
Ψ	stream function
ω	vorticity.

Energy equation

$$\frac{\partial}{\partial r}\left(C_p T \frac{\partial \psi}{\partial z}\right) - \frac{\partial}{\partial z}\left(C_p T \frac{\partial \psi}{\partial r}\right) + \frac{\partial}{\partial z}\left(rk \frac{\partial T}{\partial z}\right) + \frac{\partial}{\partial r}\left(rk \frac{\partial T}{\partial r}\right) = 0. \quad (3)$$

The stream function ψ and vorticity ω in the above equations are defined in terms of the radial velocity u and the axial velocity v as follows:

$$u = -\frac{1}{\rho_L r}\frac{\partial \psi}{\partial z}, \quad (4)$$

$$v = \frac{1}{\rho_L r}\frac{\partial \psi}{\partial r}, \quad (5)$$

$$\omega = \frac{\partial u}{\partial z} - \frac{\partial v}{\partial r}. \quad (6)$$

The thermal boundary conditions are as follows:

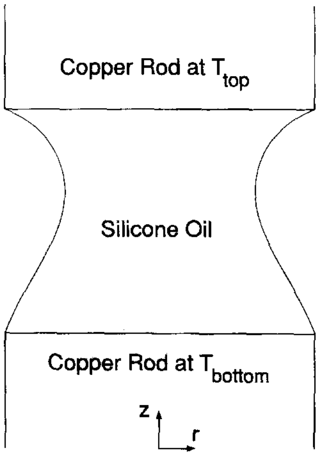

Fig. 1. Schematic sketch of the floating zone being considered.

1. along the axis,

$$\frac{\partial T}{\partial r} = 0 \text{ due to symmetry}; \quad (7)$$

2. at the top oil–solid interface,

$$T = T_{top}; \quad (8)$$

3. at the bottom oil–solid interface,

$$T = T_{bottom}; \quad (9)$$

4. at the free surface,

$$-k(\vec{n}\cdot\nabla T) = h(T - T_a) + \varepsilon\sigma(T^4 - T_a^4), \quad (10)$$

where $\vec{n}$ is the unit normal vector, pointing radially outward.

The fluid-flow boundary conditions are as follows:

1. along the axis,

$$\psi = 0 \quad (11)$$

$$\omega = 0, \quad (12)$$

the stream function is set to zero at the axis as a reference. The zero vorticity is the result of $\partial u/\partial z = \partial v/\partial r = 0$ at the axis;

2. at the oil–solid interfaces,

$$\psi = 0, \quad (13)$$

$$\omega = \frac{\partial}{\partial z}\left(\frac{-1}{\rho_L r}\frac{\partial \psi}{\partial z}\right); \quad (14)$$

3. at the free surface of the oil,

$$\psi = 0, \quad (15)$$

$$\omega = \frac{\partial u}{\partial z} - \frac{\partial v}{\partial r}, \quad (16)$$

with:

$$\vec{n}\vec{s}:\mathbf{t} = \frac{\partial \gamma}{\partial T}(\vec{s}\cdot\nabla T), \quad (17)$$

where $\vec{n}$ and $\vec{s}$ are, respectively, the unit normal vector

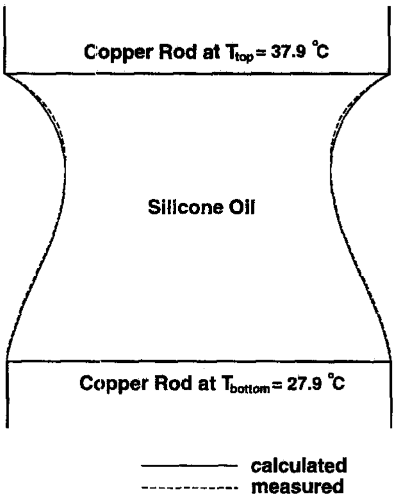

Fig. 2. A calculated free surface shape showing good agreement with the observed one.

and unit tangential vector at the free surface, $\mathbf{t}$ the stress tensor and $\partial\gamma/\partial T$ the surface tension–temperature coefficient of the oil. Equation (17) is the shear–stress balance at the free surface.

COORDINATE TRANSFORMATION

Due to the fact that the free surface is not flat but curved, the vorticity boundary condition in terms of the cylindrical coordinate system (r, z), i.e. equation (17), cannot be implemented properly. This is mainly because the free surface does not pass through the grid points. In view of this problem we have transformed the above governing equations and boundary conditions into those in terms of general (non-orthogonal) curvilinear coordinates (η, ξ) which fit all the interfaces, as shown in Fig. 2. In this way, all the boundary conditions can be treated accurately.

Following the procedure of Thompson *et al.* [54], equations (1)–(3) can be transformed into the following general form:

$$\frac{\partial}{\partial\eta}\left(a\phi\frac{\partial\psi}{\partial\xi}\right)-\frac{\partial}{\partial\xi}\left(a\phi\frac{\partial\psi}{\partial\eta}\right)+\frac{b}{J}\left[g_{22}\frac{\partial^2(c\phi)}{\partial\eta^2}+g_{11}\frac{\partial^2(c\phi)}{\partial\xi^2}\right]+d_{PQ}+d_{nor}+d_{or}=0. \quad (18)$$

Coefficients a, b, c and d in the above equation are given in Table 1 for $\phi = \psi$, ω and T, respectively.

Table 1. Coefficients a, b, c and d in equation (18)

ϕ	a	b	c	d
ψ	0	$\frac{1}{\rho_L r}$	1	ω
ω	$\frac{1}{r}$	$\frac{1}{r}$	μr	$-\frac{\rho_L g\beta}{J}\left[\frac{\partial z}{\partial\xi}\frac{\partial T}{\partial\eta}-\frac{\partial z}{\partial\eta}\frac{\partial T}{\partial\xi}\right]$
T	C_p	kr	1	0

Other coefficients in the same equation are defined as follows:

$$d_{PQ} = bJ\left[P(\eta,\xi)\frac{\partial(c\phi)}{\partial\eta}+Q(\eta,\xi)\frac{\partial(c\phi)}{\partial\xi}\right], \quad (19)$$

$$d_{nor} = -\frac{2bg_{12}}{J}\frac{\partial^2(c\phi)}{\partial\eta\,\partial\xi}+\frac{1}{J}\left[\left(g_{22}\frac{\partial b}{\partial\eta}-g_{12}\frac{\partial b}{\partial\xi}\right)\times\frac{\partial(c\phi)}{\partial\eta}+\left(g_{11}\frac{\partial b}{\partial\xi}-g_{12}\frac{\partial b}{\partial\eta}\right)\frac{\partial(c\phi)}{\partial\xi}\right], \quad (20)$$

$$d_{or} = Jd, \quad (21)$$

$$g_{11} = \left(\frac{\partial r}{\partial\eta}\right)^2+\left(\frac{\partial z}{\partial\eta}\right)^2, \quad (22)$$

$$g_{22} = \left(\frac{\partial r}{\partial\xi}\right)^2+\left(\frac{\partial z}{\partial\xi}\right)^2, \quad (23)$$

$$g_{12} = \left(\frac{\partial r}{\partial\eta}\right)\left(\frac{\partial r}{\partial\xi}\right)+\left(\frac{\partial z}{\partial\eta}\right)\left(\frac{\partial z}{\partial\xi}\right), \quad (24)$$

where:

$$J = \left(\frac{\partial r}{\partial\eta}\right)\left(\frac{\partial z}{\partial\xi}\right)-\left(\frac{\partial z}{\partial\eta}\right)\left(\frac{\partial r}{\partial\xi}\right), \quad (25)$$

$$P = \left\{g_{22}\left[\frac{\partial^2 z}{\partial\eta^2}\frac{\partial r}{\partial\xi}-\frac{\partial^2 r}{\partial\eta^2}\frac{\partial z}{\partial\xi}\right]-2g_{12}\left[\frac{\partial r}{\partial\xi}\frac{\partial^2 z}{\partial\eta\,\partial\xi}-\frac{\partial z}{\partial\xi}\frac{\partial^2 r}{\partial\eta\,\partial\xi}\right]+g_{11}\left[\frac{\partial^2 z}{\partial\xi^2}\frac{\partial r}{\partial\xi}-\frac{\partial z}{\partial\xi}\frac{\partial^2 r}{\partial\xi^2}\right]\right\}/J^3, \quad (26)$$

$$Q = \left\{g_{22}\left[\frac{\partial^2 r}{\partial\eta^2}\frac{\partial z}{\partial\eta}-\frac{\partial^2 z}{\partial\eta^2}\frac{\partial r}{\partial\eta}\right]-2g_{12}\left[\frac{\partial z}{\partial\eta}\frac{\partial^2 r}{\partial\eta\,\partial\xi}-\frac{\partial r}{\partial\eta}\frac{\partial^2 z}{\partial\eta\,\partial\xi}\right]+g_{11}\left[\frac{\partial^2 r}{\partial\xi^2}\frac{\partial z}{\partial\eta}-\frac{\partial r}{\partial\eta}\frac{\partial^2 z}{\partial\xi^2}\right]\right\}/J^3. \quad (27)$$

The transformed thermal boundary conditions are as follows:

1. along the axis,

$$\frac{\partial T}{\partial\eta} = 0; \quad (28)$$

2. at the top oil–solid interface,

$$T = T_{top}; \quad (29)$$

3. at the bottom oil–solid interface,

$$T = T_{bottom}; \quad (30)$$

4. at the free surface,

$$-k(\bar{\mathbf{n}}\cdot\nabla T) = h(T-T_a)+\varepsilon\sigma(T^4-T_a^4). \quad (31)$$

The transformed fluid-flow boundary conditions are as follows:

1. along the axis,

$$\psi = 0, \tag{32}$$

$$\omega = 0; \tag{33}$$

2. at the oil–solid interfaces,

$$\psi = 0, \tag{34}$$

$$\omega = -\frac{g_{11}}{\rho_L r J^2}\frac{\partial^2 \psi}{\partial \xi^2}; \tag{35}$$

3. at the free surface,

$$\psi = 0, \tag{36}$$

$$\omega = -\frac{1}{\mu g_{22}^{1/2}}\frac{\partial \gamma}{\partial T}\frac{\partial T}{\partial \xi} + \frac{2}{g_{22}}\left[\frac{\partial z}{\partial \xi}\frac{\partial u}{\partial \xi} - \frac{\partial r}{\partial \xi}\frac{\partial v}{\partial \xi}\right]. \tag{37}$$

Along the free surface, ψ is constant and $\partial\psi/\partial\xi = 0$. From this, it can be shown that $\vec{\mathbf{n}}\cdot(u\vec{\mathbf{e}}_r + v\vec{\mathbf{e}}_Z) = 0$. This equation is the so-called kinematic condition. The shape of the free surface is calculated from the normal stress balance at the free surface, which has already been described previously [30].

METHOD OF SOLUTION

The numerical method for solving equations (1)–(3) is similar to that of Gosman *et al.* [55] and has already been described elsewhere [56]. This method is a control-volume finite-difference method for solving governing equations in terms of the stream function and vorticity. The convergence criteria are as follows:

$$\frac{\Sigma|\psi - \psi_{\text{old}}|}{\Sigma|\psi|} < 1\times 10^{-5},$$

$$\frac{\Sigma|\omega - \omega_{\text{old}}|}{\Sigma|\omega|} < 1\times 10^{-5},$$

$$|T - T_{\text{old}}|_{\text{max}} < 1\times 10^{-4}\,^{\circ}\text{C},$$

where Σ denotes summation over all grid points, and max the maximum of all grid-point values.

EXPERIMENTAL PROCEDURE

The silicone oil used was Dow Corning Fluid 200, 5.0 cs. Two copper rods close to 0.4 cm (actually 0.412 cm) in diameter were prepared. In previous experimental studies, copper or aluminum rods, 0.3 or 0.4 cm in diameter, were very often used, since fluid flow in a silicone oil zone of this small size is dominated by thermocapillary flow rather than natural convection. Consequently, thermocapillary flow can be studied under normal gravity.

The temperature of each rod was kept constant during the experiment with the help of a thermocouple located near the oil end of the rod. The thermocouple was connected to a temperature controller which regulated the heater power.

Two different experiments were conducted. In the first case, the temperatures of the upper and lower rods were 31.0 and 20.8°C, respectively, and the gap between the rods was 0.303 cm. In the second case, these values became 37.9°C, 27.8°C and 0.306 cm, respectively. In both cases, the oil zone was not cylindrical in shape but necked significantly. The zone collapsed when more silicone oil was added to reduce necking. Such necking has been reported previously in similar floating zones [37, 40, 41].

Flow visualization was conducted using a laser light-cut technique, which has been described elsewhere [49]. In brief, small marker particles of aluminum were added to the silicone oil to help reveal the flow patterns. A thin (about 0.5 mm) vertical sheet of He–Ne laser light was caused to cut the oil zone through its meridian plane, to illuminate the moving particles in the plane. In both cases, convection was stable and axisymmetric.

RESULTS AND DISCUSSION

The physical properties of 5 cs silicone oil are given in Table 2 [57, 58]. Recent measurements [58] showed that $\partial\gamma/\partial T = -0.062$ and -0.060 dyne cm^{-1} °C^{-1} for 2 and 10 cs silicone oils, respectively. As such, -0.060 dyne cm^{-1} °C^{-1} was taken as the $\partial\gamma/\partial T$ value for 5 cs silicone oil. The refractive index $n = 1.396$. Heat losses from the free surface are neglected since the temperatures of the copper rods are close to the room temperature.

An example of the calculated shapes of the free surface is shown in Fig. 2. As shown, the agreement between the calculated and observed free surfaces is very good.

An example of the grids used for computation is shown in Fig. 3. As shown, the grid spacing is non-uniform, i.e. finer near the free surface and the oil–solid interfaces, where temperature and velocity gradients are expected to be greater. This grid system has 31×41 grid points in the oil zone and further reduction in grid spacing did not produce significant differences. The same grid system was used in our previous studies on floating-zone crystal growth [29–32] where the effect of grid spacing was already discussed in detail.

Figure 4 shows the calculated result for the case where the upper and lower copper rods are kept at 31.0 and 20.8°C, respectively. As expected from the

Table 2. Physical properties of 5 cs silicone oil [57, 58]

$k_L = 1.09\times 10^{-3}$ W cm^{-1} °C^{-1}
$C_p = 1.714$ J g^{-1} °C^{-1}
$\beta = 1.05\times 10^{-3}$ °C^{-1}
$\partial\gamma/\partial T = -0.060$ dyne cm^{-1} °C^{-1}
$\gamma = 18.7 + (T - 25°\text{C})\partial\gamma/\partial T$ dyne cm^{-1}
$\mu = 0.04565$ g cm^{-1} s^{-1}
$\rho_L = 0.913$ g cm^{-3}
$n = 1.396$

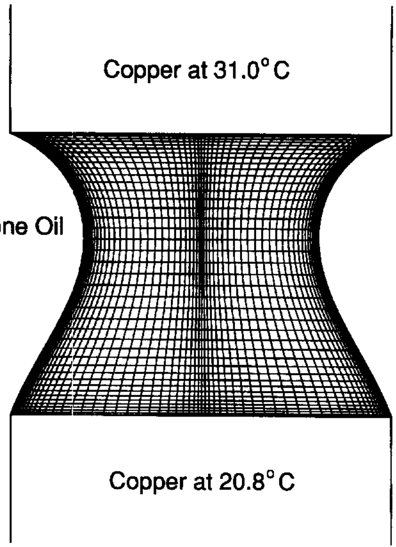

Fig. 3. A grid mesh used for computations of heat transfer and fluid flow in the floating zone.

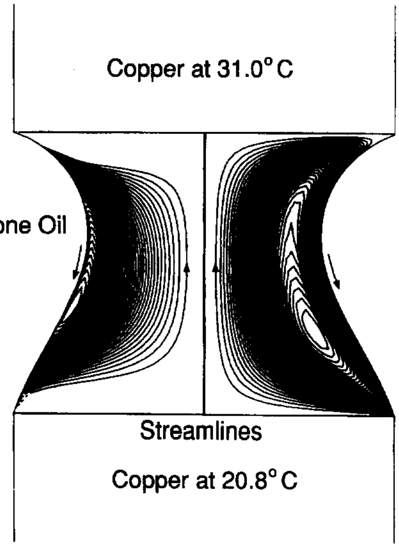

Fig. 5. The flow pattern (left), for the case of $T_{top} = 31.0°C$ and $T_{bottom} = 20.8°C$, based on the calculated streamlines (right) and the lens effect of the oil zone.

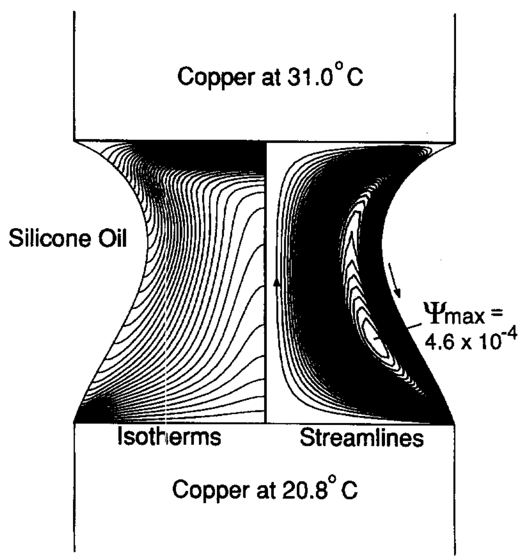

Fig. 4. Calculated results for the case of $T_{top} = 31.0°C$ and $T_{bottom} = 20.8°C$: isotherms (left) and streamlines (right).

negative $\partial\gamma/\partial T$ value of the silicone oil, the calculated streamlines show that the oil flows along the free surface from the hotter rod at the top (where the surface tension is lower) to the cooler rod at the bottom (where the surface tension is higher). The liquid then turns around and flows inward and upward back to the hotter rod at the top. The maximum stream function is $\psi_{max} = 4.6 \times 10^{-4}$ g s^{-1}. The streamlines are evenly spaced at $\Delta\psi = (\psi_{max} - 0)/40$. The maximum velocity is 0.347 cm s^{-1} and is located near the bottom of the free surface.

The calculated isotherms are shown at the interval of $\Delta T = (T_{top} - T_{bottom})/40$. As expected from the rather high Prandtl number (71.8) of the silicone oil, the isotherms are significantly distorted, i.e. being pushed downward along the free surface and upward along the axis.

Figure 5 shows the flow pattern (LHS) which is converted from the calculated streamlines (RHS) following the procedure described in ref. [53] to incorporate the lens effect of the oil zone. As compared to the as-calculated streamlines, the lens effect of the oil zone causes the streamlines to appear to shift toward the free surface and away from both oil–solid interfaces. It also causes the vortex to appear to shift outward and upward. It was observed that with severe zone necking converted streamlines near the lower and upper corners of the free surface can jump due to singularity and need to be smoothed.

Figure 6 shows the comparison between the calculated and observed flow patterns. The wiggling in the flow lines was caused by unintentional camera vibration during photographing. This problem was corrected in a subsequent experiment by holding down the camera to a heavy stable base. As shown, the calculated and converted flow pattern agrees very well with the observed one. The location of the calculated and converted vortex is very close to that of the observed one. The centers of the two vortices are about the same distance both from the lower copper rod and from the free surface. Both flow patterns show no visible streamlines in the areas near the oil–solid interfaces. The 'ghost' streamlines visible near the lower copper rod are just the free-surface reflection of the streamlines from above. In fact, some clusters of aluminum particles resting at the bottom of the oil zone are also visible near the oil–solid interfaces.

Figure 7 shows the calculated result for the case where the upper and lower copper rods are kept at 37.9 and 27.8°C, respectively. The streamlines and isotherms are similar to those shown in Fig. 4. The maximum stream function $\psi_{max} = 5.0 \times 10^{-4}$ g s^{-1}.

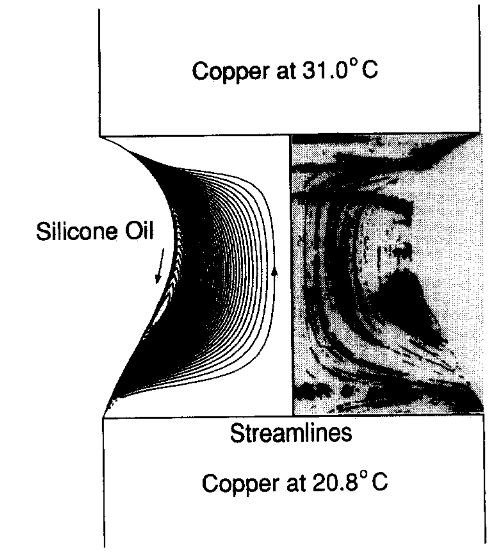

Fig. 6. Comparison, for the case of $T_{top} = 31.0°C$ and $T_{bottom} = 20.8°C$, between the calculated (left) and observed (right) flow patterns.

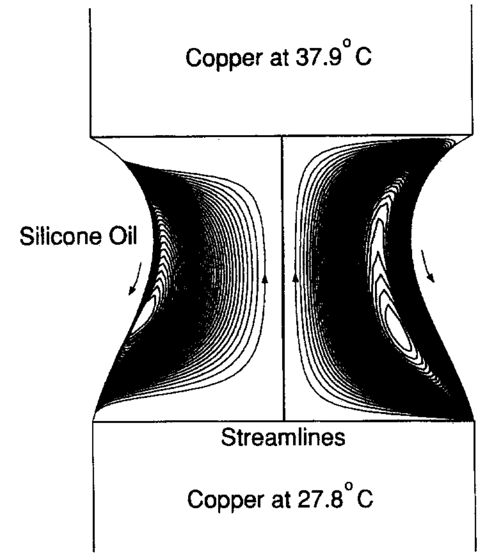

Fig. 8. The flow pattern (left), for the case of $T_{top} = 37.9°C$ and $T_{bottom} = 27.8°C$, based on the calculated streamlines (right) and the lens effect of the oil zone.

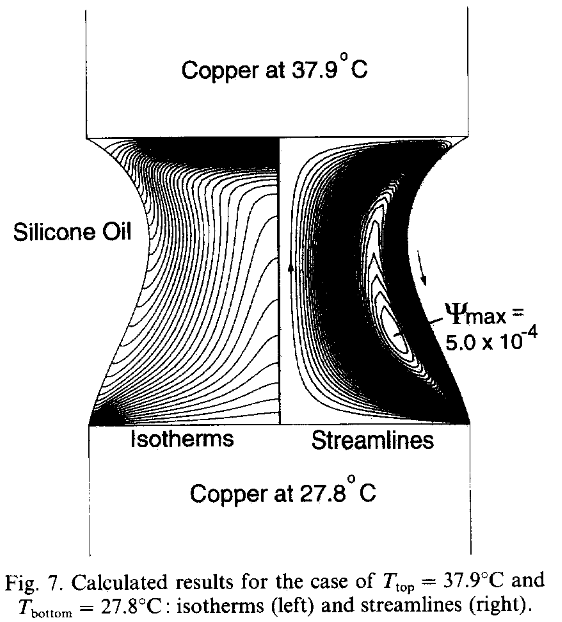

Fig. 7. Calculated results for the case of $T_{top} = 37.9°C$ and $T_{bottom} = 27.8°C$: isotherms (left) and streamlines (right).

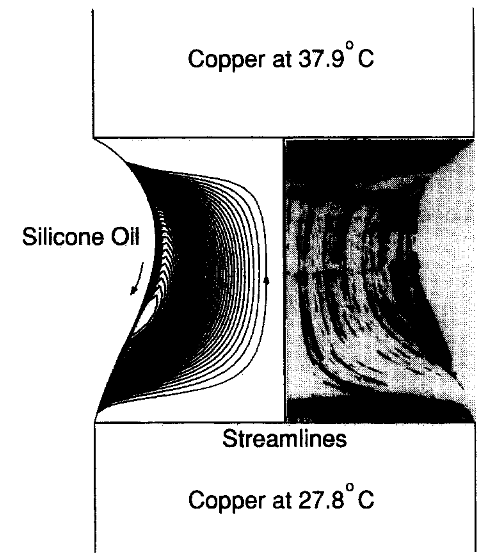

Fig. 9. Comparison, for the case of $T_{top} = 37.9°C$ and $T_{bottom} = 27.8°C$, between the calculated (left) and observed (right) flow patterns.

The maximum velocity is 0.377 cm s^{-1} and is again located near the bottom of the free surface.

As shown in Fig. 8, the lens effect of the oil zone again causes the streamlines to appear to shift toward the free surface and away from the oil–solid interfaces. It also appears to shift the vortex upward and outward again.

As shown in Fig. 9, the calculated and converted flow pattern is again in very good agreement with the observed one.

Quantitative comparison between calculated and converted velocity fields with measured ones is underway and will be reported subsequently.

CONCLUSIONS

Thermocapillary flow in a silicone oil floating zone has been studied by computer simulation and flow visualization. The lens effect due to the noncylindrical shape of the floating zone causes the streamlines to appear to shift toward the free surface and away from the top and bottom of the zone. It also causes the vortex to appear to shift outward and upward. By incorporating the lens effect, the calculated streamlines have been converted to flow patterns that can be compared with the observed ones from flow visualization. The calculated and converted flow patterns are in very good agreement with the observed ones.

Acknowledgement—This study was supported by NASA under Grant No. NAG-1393.

REFERENCES

1. G. H. Harriott and R. A. Brown, Steady solute fields induced by differential rotation in small floating zone, *J. Crystal Growth* **69,** 589–604 (1984).
2. J. Y. Murthy, A numerical simulation of flow, heat and mass transfer in a floating zone at high rotational Reynolds numbers, *J. Crystal Growth* **83,** 23–34 (1987).
3. J. Y. Murthy, The influence of secondary convection on axial segregation in a floating zone, *Trans. ASME* **110,** 662–669 (1988).
4. N. Kobayashi, Computer simulation of the steady flow in a cylindrical floating zone under microgravity, *J. Crystal Growth* **66,** 63–72 (1984).
5. B. Fu and S. Ostrach, Numerical solutions of thermocapillary flows in floating zones. In *Transport Phenomenon in Materials Processing*, pp. 1–9. ASME (1983).
6. Y. Kamotani, S. Ostrach and M. Vargas, Oscillatory thermocapillary convection in a simulated floating-zone configuration, *J. Crystal Growth* **66,** 83–90 (1984).
7. S. Ostrach, Y. Kamotani and C. I. Lai, Oscillatory thermocapillary flows, *Chem. Hydrodyn.* **6,** 585–559 (1985).
8. P. A. Clark and W. R. Wilcox, Influence of gravity on thermocapillary convection in floating zone melting of silicon, *J. Crystal Growth* **50,** 461–469 (1980).
9. C. Chang and W. R. Wilcox, Inhomogeneities due to thermocapillary flow in floating zone melting, *J. Crystal Growth* **28,** 8–12 (1975).
10. C. Chang and W. R. Wilcox, Analysis of surface tension driven flow in floating zone melting, *Int. J. Heat Mass Transfer* **19,** 355–366 (1976).
11. N. Kobayashi and W. R. Wilcox, Computational studies of convection due to rotation in a cylindrical floating zone, *J. Crystal Growth* **59,** 616–624 (1982).
12. A. Rybicki and J. M. Floryan, Thermocapillary effects in liquid bridges. I—Thermocapillary convection, II—Deformation of the interface and capillary instability, *Phys. Fluids* **30,** 1956–1972, 1973–1983 (1987).
13. R. Natarjan, Thermocapillary flows in a rotating float zone under microgravity, *A.I.Ch.E. Jl* **35,** 614–624 (1989).
14. L. G. Napolitano, C. Golia and A. Viviani, Effects of variable transport properties on thermal Marangoni flows, *Acta Astronaut.* **13,** 661–667 (1986).
15. L. G. Napolitano, C. Golia and A. Viviani, Numerical simulation of unsteady thermal Marangoni flows, *Proceedings of 5th European Symposium on Materials Science under Microgravity*, Schloss Elmau (1984).
16. Z. Kozhoukharova and S. Slavchev, Computer simulation of the thermocapillary convection in a non-cylindrical floating zone, *J. Crystal Growth* **74,** 236–246 (1986).
17. W. W. Fowlis and G. O. Roberts, Confinement of thermocapillary floating zone flow by uniform rotation, *J. Crystal Growth* **74,** 301–320 (1986).
18. M. K. Smith, Thermocapillary and centrifugal-buoyancy driven motion in a rapidly rotating liquid cylinder, *J. Fluid Mech.* **166,** 245–264 (1986).
19. K. H. Lie, D. N. Riahi and J. S. Walker, Buoyancy and surface tension driven flows in float zone crystal growth with a strong axial magnetic field, *Int. J. Heat Mass Transfer* **32,** 2409–2420 (1989).
20. D. N. Riahi and J. S. Walker, Float zone shape and stability with electromagnetic body force due to a radiofrequency induction coil, *J. Crystal Growth* **94,** 635–642 (1989).
21. K.-H. Lie, J. S. Walker and D. N. Riahi, Centrifugal pumping in the float zone growth of silicon crystals with an axial magnetic field, *PhysicoChem. Hydrodyn.* **10,** 441–460 (1988).
22. R. Rupp, G. Muller and G. Neumann, Three-dimensional time dependent modelling of the Marangoni convection in zone melting configurations of GaAs, *J. Crystal Growth* **97,** 34–41 (1989).
23. A. Mulbeauer and W. Erdmann, Electrodynamic convection in silicon floating zones, *J. Crystal Growth* **64,** 529–545 (1983).
24. Y. Shen, G. P. Neitzel, D. F. Jankowski and H. D. Mittelmann, Energy stability of thermocapillary convection in a model of the float-zone crystal-growth process, *J. Fluid Mech.* **217,** 639–660 (1990).
25. J. R. Hyer, D. F. Jankowski and G. P. Neitzel, Thermocapillary convection in a model float zone, *J. Thermophys.* **5,** 577–582 (1991).
26. J. L. Duranceau and R. A. Brown, Thermal-capillary analysis of small scale floating zones: steady-state calculations, *J. Crystal Growth* **75,** 367–389 (1986).
27. G. W. Young and A. Chait, Steady-state thermal–solutal diffusion in a float zone, *J. Crystal Growth* **96,** 65–95 (1989).
28. G. W. Young and A. Chait, Surface tension driven heat, mass and momentum transport in a two-dimensional float-zone, *J. Crystal Growth* **106,** 455–466 (1990).
29. C. W. Lan and S. Kou, Thermocapillary flow and melt/solid interfaces during floating-zone crystal growth under microgravity, *J. Crystal Growth* **102,** 1043–1058 (1990).
30. C. W. Lan and S. Kou, Heat transfer, fluid flow and interface shapes in floating-zone crystal growth, *J. Crystal Growth* **108,** 351–366 (1991).
31. C. W. Lan and S. Kou, Effects of rotation on heat transfer, fluid flow and interfaces in normal gravity floating zone crystal growth, *J. Crystal Growth* **114,** 517–535 (1991).
32. C. W. Lan, S. Kou and B. C. Liao, Effect of rotation on microgravity floating-zone crystal growth, *8th European Symposium on Materials and Fluid Sciences in Microgravity*, Brussels, p. 103. ESA SP-333 (1992).
33. B. Xiong and W. R. Hu, Crystal growth in floating zone with phase change and thermo-solutal convections, *J. Crystal Growth* **125,** 149–163 (1992).
34. B. Xiong and W. R. Hu, Influence of low-gravity level on crystal growth in floating zone, *J. Crystal Growth* **133,** 155–167 (1993).
35. C. W. Lan and S. Kou, Radial segregation in zero-gravity floating-zone crystal growth, *J. Crystal Growth* **132,** 578–591 (1993).
36. C. W. Lan and S. Kou, Effect of rotation on radial dopant segregation in microgravity floating zone crystal growth, *J. Crystal Growth* **133,** 309–321 (1993).
37. C.-H. Chun and W. Wuest, A micro-gravity simulation of the Marangoni convection, *Acta Astronaut.* **5,** 681–686 (1978).
38. C.-H. Chun and W. Wuest, Experiments on transition from the steady to oscillatory Marangoni-convection of a floating zone under reduced gravity effect, *Acta Astronaut.* **6,** 1073–1082 (1979).
39. C.-H. Chun and W. Wuest, Suppression of temperature oscillations of thermal Marangoni convection in a floating zone by superimposing of rotating flows, *Acta Astronaut.* **9,** 225–230 (1982).
40. C.-H. Chun, Marangoni convection in a floating zone under reduced gravity, *J. Crystal Growth* **48,** 600–610 (1980).
41. C.-H. Chun, Experiments on steady and oscillatory temperature distribution in a floating zone due to the Marangoni convection, *Acta Astronaut.* **7,** 479–488 (1980).
42. S. Ostrach, Y. Kamotani and J. Lee, Oscillatory thermocapillary flows, *Adv. Space Res.* **13,** 97–104 (1993).
43. D. Schwabe, A. Scharmann and F. Preisser, Steady and oscillatory Marangoni convection in floating zones

under 1-g, *Proceedings of 3rd European Symposium on Materials Sciences in Space*, Grenoble, p. 327. ESA-142 (1979).
44. D. Schwabe, A. Scharmann, F. Preisser and R. Oeder, Marangoni convection in floating zones, *Proceedings of 3rd European Symposium on Materials Sciences in Space*, Grenoble, p. 333. ESA-142 (1979).
45. F. Preisser, D. Schwabe and A. Scharmann, Steady and oscillatory thermocapillary convection in liquid columns with free cylindrical surface, *J. Fluid Mech.* **126,** 545–567 (1983).
46. D. Schwabe, A. Scharmann, F. Priesser and R. Oeder, Experiments on surface tension driven flow in floating zone melting, *J. Crystal Growth* **43,** 305–312 (1978).
47. C. W. Lan and S. Kou, A simple method for improving stability of a floating melt zone, *J. Crystal Growth* **118,** 151–159 (1992).
48. C. W. Lan and S. Kou, Shortened floating zone crystal growth, *J. Crystal Growth* **119,** 281–291 (1992).
49. C. W. Lan, Y. J. Kim and S. Kou, A half-zone study of Marangoni convection in floating-zone crystal growth under microgravity, *J. Crystal Growth* **104,** 801–808 (1990).
50. D. Schwabe and A. Scharmann, Marangoni convection in open boat and crucible, *J. Crystal Growth* **52,** 435–449 (1981).
51. C.-H. Chun, Numerical study on the thermal Marangoni convection and comparison with experimental results from the Texas-rocket program, *Acta Astronaut.* **11,** 227–232 (1984).
52. T. Surek and B. Chalmers, The direction of growth of the surface of a crystal in contact with its melt, *J. Crystal Growth* **29,** 1–11 (1975).
53. C. W. Lan and S. Kou, Formulation for correcting optical distortions due to a transparent floating zone, *J. Crystal Growth* **132,** 471–476 (1993).
54. J. F. Thompson, F. C. Thames and C. W. Mastin, Boundary-fitted curvlinear coordinate for solution of partial differential equations on fields containing any number of arbitrary 2-dimensional bodies, NASA Report: NASA-CR-2729 (1977).
55. A. D. Gosman, W. M. Pan, A. K. Runchal, D. B. Spalding and M. Wolfshtein, *Heat and Mass Transfer in Recirculating Flows*, pp. 18–115. Academic Press, London (1969).
56. C. W. Lan and S. Kou, Thermocapillary flow and natural convection in a melt column with an unknown melt/solid interface, *Int. J. Numer. Meth. Fluids* **12,** 59–80 (1991).
57. *Information about Dow Corning Silicone Fluids*. Dow Corning, Midland, MI (1990).
58. Jean N. Koster, Private communication, University of Colorado, Boulder, CO (1993).